Journal of Alloys and Compounds 495 (2010) 224–228

Contents lists available at ScienceDirect

Journal of Alloys and Compounds

journal homepage: www.elsevier.com/locate/jallcom

Microstructure evolution in Nd:YAG laser-welded $(Zr_{53}Cu_{30}Ni_9Al_8)Si_{0.5}$ bulk metallic glass alloy

Huei-Sen Wang[a,*], Hou-Guang Chen[a], Jason Shian-Ching Jang[b]

[a] Department of Materials Science and Engineering, I-Shou University, Kaohsiung 840, Taiwan
[b] Department of Mechanical Engineering, National Central University, Taoyuan County 32001, Taiwan

ARTICLE INFO

Article history:
Received 22 July 2009
Received in revised form 25 January 2010
Accepted 28 January 2010
Available online 4 February 2010

Keywords:
(Zr53Cu30Ni9Al8)Si0.5
Bulk metallic glass
Nd:YAG laser welding

ABSTRACT

To generate a rapid welding thermal cycle for a $(Zr_{53}Cu_{30}Ni_9Al_8)Si_{0.5}$ bulk metallic glass (BMG) weld, the Nd:YAG pulse laser welding process with pre-selected welding variables is used in this study. The microstructure development and crystallization behavior in the weld fusion zone (WFZ) and the heat-affected zone (HAZ) are investigated by scanning electron microscopy (SEM), micro-area X-ray diffractometry (XRD) and transmission electron microscopy (TEM). From the results, it is observed that the HAZ is liable to crystallize, although no crystallization occurs within the WFZ. The spherical type crystalline phases (with a particle size of 20–200 nm) observed in the HAZ, which are rich in Zr, Cu and Ni, result in a change of chemical composition in this region. Furthermore, if the particle size in the crystallized area is greater than 50 nm, cracks may form.

1. Introduction

Zr-based bulk metallic glass (BMG) has received considerable attention in studies [1–11] of amorphous alloys due to its wide supercooled liquid region and high glass forming ability (GFA) among the alloy systems. However, as with other BMGs, Zr-based BMG has major problems in terms of practical applications, product size for structural use and phase stability [4,6,12–15] during the working processes. In order to extend the engineering applications for Zr-based BMG, specific welding technologies need to be developed. To successfully weld a BMG, extremely rapid solidification or thermal quench in the weld fusion zone (WFZ) or the heat-affected zone (HAZ) must be generated. Recent developments in Zr-based BMG welding have seen the use of five methods: the spark [6], explosion [6], high power fiber laser [11], electron beam [9,10] and friction [13,16,17] welding processes.

Several articles have also recently focused on the study of Cu-based BMG joining with pulse Nd:YAG [18] (neodymium doped yttrium aluminum garnet) laser welding because of its advantages of higher welding energy density and deeper penetration. For Zr-based BMG, Nd:YAG has been successfully used for the surface modification [19]; however, to date, only few attempts [20] have been made at Nd:YAG laser welding for Zr-based BMG. Therefore, in this study, a $(Zr_{53}Cu_{30}Ni_9Al_8)Si_{0.5}$ amorphous alloy, which was computationally designed by thermodynamics and deep eutectic methodology [21,22], was employed for welding using the Nd:YAG process with pre-selected welding parameters. After the welding, the microstructure development and crystallization behavior in the weld metal and the HAZ were investigated.

2. Experimental procedures

$(Zr_{53}Cu_{30}Ni_9Al_8)Si_{0.5}$ BMG plates 1 mm in thickness, 20 mm in width and 30 mm in length, machined from the cast plates, were prepared for Nd:YAG laser welding. The test plates were all polished with 1000-grit SiC paper to remove existing surface oxides. Welds by the bead-on-plate (BOP) method were conducted using three laser welding conditions, as summarized and shown in Table 1. To avoid the crystallization in the welds, welding parameters (including pulse peak power, pulse duration and pulse frequency) were pre-selected in reference to an earlier study [16] and based on the empirical approach, with the emphasis on the possible minimum energy required to penetrate the 1 mm BMG plates. During the welding process, the top and bottom surfaces of the test plates were shielded by pure argon to prevent surface oxidation.

The polished plate was etched in a solution of 100 ml H_2O, 5 ml H_2O_2 and 2 ml HF. The weld microstructure was observed by scanning electron microscopy (SEM). The distribution of chemical elements in the WFZ and HAZ was determined by energy dispersive X-ray spectroscopy (EDS). The glassy structure was identified by micro-area X-ray diffractometry (XRD, Scintag X-400 X-ray diffractometer) using Cu K radiation and transmission electron microscopy (Philip Tecnai G2 TEM).

3. Results

With the BOP method, which is produced by moving and periodic irradiated laser energy, each position of the weld suffers different thermal cycles (according to heating rate, peak temperature and cooling rate). As a result, a welded BMG is composed of the WFZ, HAZ and unaffected base material. Given their contrastive differences, the WFZ, HAZ and unaffected parent material

* Corresponding author. Tel.: +886 7 6577711x3111; fax: +886 7 6578444.
E-mail address: hueisen2000@hotmail.com (H.-S. Wang).

0925-8388/$ – see front matter © 2010 Elsevier B.V. All rights reserved.
doi:10.1016/j.jallcom.2010.01.132

Table 1
Welding parameters for BMG plates.

No.	Peak power (kW)	Pulse duration (ms)	Laser energy (J)	Frequency (Hz)	Travel speed (mm/min)	Spot size (mm)
A	1.7	5.9	7.0	2	60	0.4
B	1.5	5.0	6.2	2	60	0.4
C	1.3	4.5	5.5	2	60	0.4

(PM) can be approximately defined. Fig. 1 shows the etched planar views of the welded BMG plates. The weld morphologies indicated that the bead width was proportional to the energy input. Fig. 1(a)–(c) show the planar sections of the weld beads which were polished to a depth of 0.07 mm. The XRD pattern (Fig. 2) of each weld showed only a broad halo diffraction pattern of 35–45° which indicated the amorphous nature of the alloy. When the planar sections were polished to a depth of 0.2 mm (see Fig. 1(d)–(f)), the marked contrasts indicated that crystallization possibly surrounded every single pulsed weld. To confirm whether or not crystallization had occurred in the WFZ of the single pulsed weld, TEM was conducted. For Sample A, which had the highest energy input and of the welds, was the most liable to crystallize, crystallization was observed in the HAZ (see Fig. 3a); however there was no crystallization in the WFZ central area (see Fig. 3b). Moreover, the WFZ central area was crystallization-free, as observed in Sample B (see Fig. 3c) and Sample C (see Fig. 3d).

A lower magnification of SEM images (see Fig. 4) showed spherical type precipitates in the HAZ from the welded plates. When the power energy increased, it was observed that the size and the amount of spherical type precipitates in the HAZ increased. EDS analysis of these precipitates in each tested plate is given in Table 2, and the analysis indicated that the precipitates were

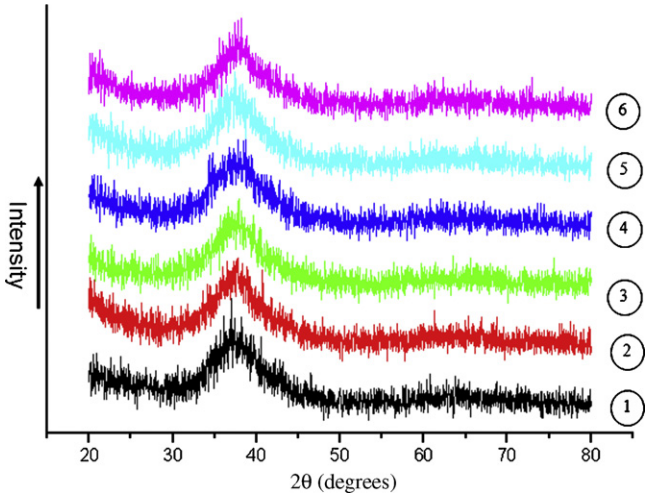

Fig. 2. The micro-focused XRD pattern of weld beads polished to a depth of 0.07 mm. The numbers indicate the corresponding areas where the XRD patterns are taken as shown in Fig. 1(a)–(c).

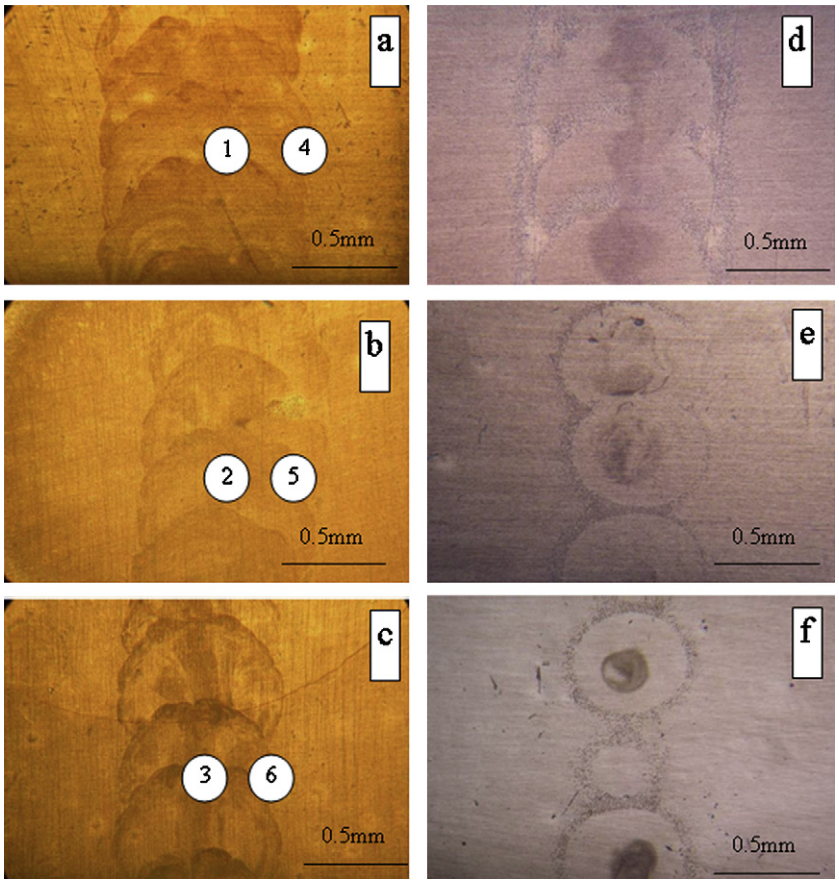

Fig. 1. Planar sections of the weld polished to a depth of 0.07 mm. The figures are taken from (a) Sample A, (b) Sample B and (c) Sample C. For the planar sections polished to a depth of 0.2 mm, the figures are taken from (d) Sample A, (e) Sample B and (f) Sample C.

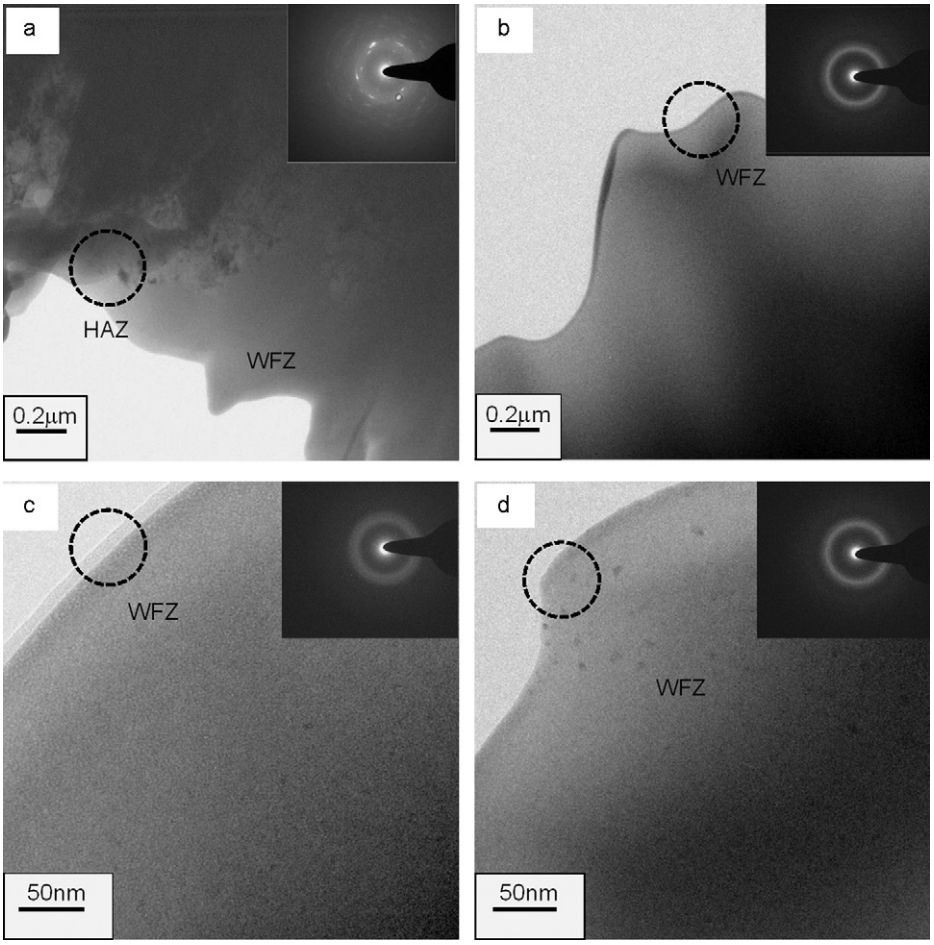

Fig. 3. TEM bright-field images and selected area diffraction patterns for (a) HAZ in Sample A (b) central area of WFZ in Sample A (d) central area of WFZ in Sample B (c) central area of WFZ in Sample C.

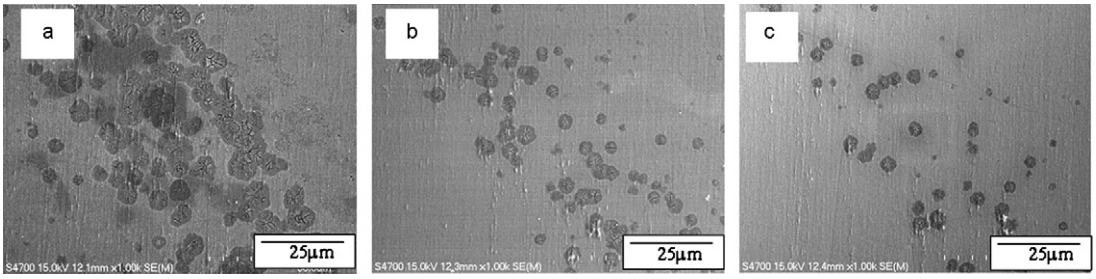

Fig. 4. A low magnification of SEM images showed spherical type precipitates in the HAZ from (a) Sample A (b) Sample B (c) Sample C.

all rich in Cu, Zr, and Ni. In addition, the chemical composition within the WFZ was not substantially affected by the intensive laser energy.

Fig. 5(a) shows a higher magnification of spherical type precipitates in the HAZ and further reveals the crystalline phases in the precipitates with a particle size of 30–200 nm (see Fig. 5b). The particle size of the crystalline phases in the precipitate surroundings approximated 20–30 nm (see Fig. 5c). Moreover, it was observed that cracks formed in the central area of the precipitates where the particle size of the crystalline phases was more than 50 nm.

Table 2
Semi-quantitative analysis of crystalline in the WFZ and HAZ by EDS (atomic %).

Sample	Region	Zr	Ni	Cu	Al
A	Precipitates in the HAZ	28.60	15.79	50.89	4.72
B	Precipitates in the HAZ	36.62	13.15	45.33	4.91
C	Precipitates in the HAZ	39.91	14.45	41.60	4.04
A	WFZ	52.59	11.80	26.95	8.66
B	WFZ	51.08	13.06	26.93	8.93
C	WFZ	54.19	11.04	27.72	7.05
PM	Unaffected zone	51.91	9.5	31.32	7.26

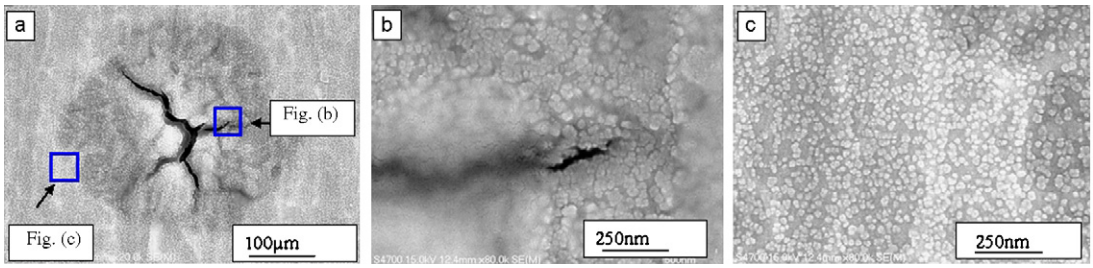

Fig. 5. (a) Higher magnification of spherical type precipitates; (b) crystalline phases in the central area of the precipitates with a particle size of 30–200 nm; and (c) crystalline particles in the HAZ with a particle size of 20–30 nm.

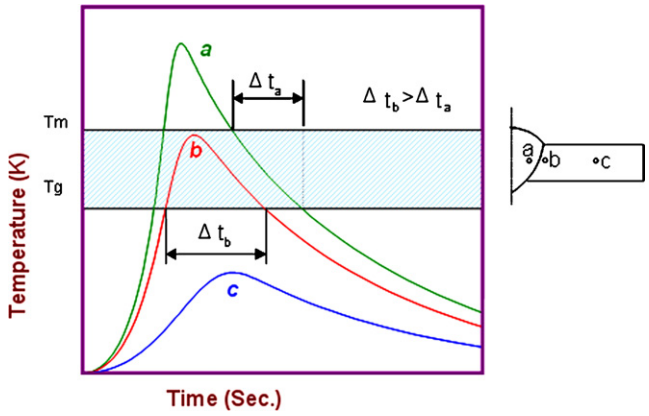

Fig. 6. Schematic representation of temperature/time profiles for WFZ (Line a) and HAZ (Line b) in the welding thermal cycles.

4. Discussion

The crystallization mechanisms in the weld metal and the HAZ were different. In terms of welding thermal cycles, a schematic representation of the temperature/time profiles for the WFZ and HAZ is shown in Fig. 6 [12]. As shown in this figure, when a supercooled liquid phase welding process (e.g. Nd:YAG laser welding) is conducted, due to its high-density energy applied to a localized area; the thermal cycle (Line "a") in WFZ is achieved easily through the liquid phase. When the weld metal is solidified from the liquid, the cooling rate ($R_{\Delta T_m/T_g}$) between melting temperature (ΔT_m) and glass transition temperature (ΔT_g) [16] is a crucial factor. If a higher energy input is provided, i.e. if the cooling rate ($R_{\Delta T_m/T_g}$) is slower than the critical cooling rate (Rc), it is possible to cool down with intercept to the crystallization nose curve. If the weld metal comes to crystallization caused by the above effects, crystallization should widely distribute over the WFS. However, in this study, the crystallization just surrounded the pulsed weld. Therefore, this implied that crystallization in the BMG WFS may have behaved differently from the above effects in this study.

For a single pulse irradiation, with the BMG HAZ basically in a solid state, the peak temperature in a welding thermal cycle was below the melting temperature (see Line "b", Fig. 5) and much lower than the WFZ, but the retention time in the crystallization temperature range, $\Delta T_m/T_g$, was longer than the WFS which was liable to crystallize in the area of the parent material HAZ (PMHAZ) [12].

For multi-pulse irradiation, two types of HAZ needed to be considered during the pulsed laser welding process: PMHAZ, the parent material region just next to the weld fusion line; and WFZHAZ, the region within the WFZ. Fig. 7 shows the schematic representation of pulse-to-pulse interaction from the multi-pulse laser welding process. As the pulse-to-pulse interactions were conducted, the first irradiation was reheated by the second irradiation. Such a reheat effect could result in an HAZ in the previous pulse weld metal (region "A") where the precipitates could be observed [16]. As the third irradiation was conducted, partial precipitates in the second irradiation (region "B") were re-melted to the liquid phase and then fast cooled without intercept to the crystallization nose curve. Therefore, the initial precipitates in region B vanished.

From the SEM and EDS analyses in the HAZ, most of the amorphous matrix was converted into the small crystalline phases, which were rich in Cu, Zr, and Ni. It was also observed that cracks formed in the central area of the precipitates. Earlier studies indicated [18] that when BMG crystallized, the volume of the crystallized region decreased because the crystallized structure was denser than the amorphous structure; thus, both the crystallized region and its surroundings were under the stressed condition. As the crystalline phases grew, this effect became more significant; moreover, if the stress exceeded the strength, cracks would occur (see Fig. 5).

5. Conclusions

A weld of $(Zr_{53}Cu_{30}Ni_9Al_8)Si_{0.5}$ bulk metallic glass (BMG) was fabricated in this study by means of the Nd:YAG pulse laser welding process. After the welding, the microstructure development and crystallization behavior in the WFZ and HAZ were investigated. The results were as follows:

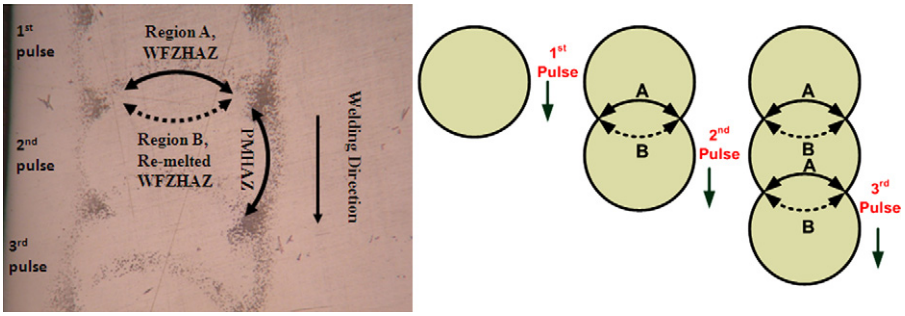

Fig. 7. Schematic representation of pulse-to-pulse interaction from the multi-pulse laser welding process.

(1) Two types of HAZ need to be considered during the pulsed laser welding process: PMHAZ, the parent material region just next to the weld fusion line; and WFZHAZ, the region within the WFZ.
(2) The HAZ was liable to crystallize when compared to the WFZ. It was observed that HAZ crystallization was inevitable.
(3) In the HAZ, most of the amorphous matrix was converted into small spherical type precipitates, which were rich in Zr, Ni and Cu.
(4) The crystalline phases in the precipitates had a particle size of 30–200 nm. The particles size of the crystalline phases in the precipitate surroundings was approximately 20–30 nm.
(5) Cracks formed in the central area of the precipitates where the particle size of the crystalline phases was more than 50 nm.

References

[1] C. Li, J. Saida, A. Inoue, Scr. Mater. 42 (2000) 1077.
[2] C. Li, J. Saida, M. Matsushid, A. Inoue, Mater. Lett. 44 (2000) 80.
[3] C. Fan, M. Imafuku, H. Kurokawa, A. Inoue, Scr. Mater. 44 (2001) 1993.
[4] E. Matsubar, M. Sakurai, T. Nakamur, M. Imafuku, S. Sato, J. Saida, A. Inoue, Scr. Mater. 44 (2001) 2297.
[5] M. Bakkal, A.J. Shih, R.O. Scattergood, Int. J. Mach. Tool Manuf. 44 (2004) 915.
[6] S. Kagao, Y. Kawamura, Y. Ohno, Mater. Sci. Eng. A 375/377 (2004) 312.
[7] J.S.C. Jang, S.F. Tsao, L.J. Chang, G.J. Chen, J.C. Huang, J. Non-Cryst. Solids 352 (2006) 71.
[8] H.S. Shin, Y.J. Jeong, H.Y. Choi, H. Kato, A. Inoue, J. Alloys Compd. 434/435 (2007) 102.
[9] J. Kim, Y. Kawamura, Scr. Mater. 56 (2007) 709.
[10] J. Kim, Y. Kawamura, J. Mater. Proc. Technol. 207 (2008) 112.
[11] Y. Kawahito, T. Terajima, H. Kimura, T. Kuroda, K. Nakata, S. Katayama, A. Inoue, Mater. Sci. Eng. B 148 (2008) 105.
[12] S. Kou, Welding Metallurgy, second ed., John Wiley & Sons, Inc., New Jersey, 2003.
[13] Y. Kawamura, T. Shoji, Y. Ohno, J. Non-Cryst. Solids 317 (2003) 152.
[14] Y. Kawamura, Mater. Sci. Eng. A 375–377 (2004) 112.
[15] T. Shoji, Y. Kawamura, Y. Ohnob, Mater. Sci. Eng. A 375/377 (2004) 394.
[16] D. Wang, B.L. Xiao, Z.Y. Ma, H.F. Zhang, Scr. Mater. 60 (2009) 112.
[17] H.S. Shina, J.S. Park, Y.C. Jung, J.H. Ahn, Y. Yokoyama, A. Inoue, J. Alloys Compd. 483 (2009) 182.
[18] J. Kim, D. Lee, S. Shin, C. Lee, Mater. Sci. Eng. A 434 (2006) 194.
[19] N.H. Tariq, B.A. Hasan, J.I. Akhter, J. Alloys Compd. 485 (2009) 212.
[20] C. Xia, L. Xing, W.Y. Long, Z.Y. Li, Y. Li, J. Alloys Compd. 484 (2009) 698.
[21] J.S.C. Jang, S.F. Tsao, L.J. Chang, J.C. Huang, C.T. Liu, Intermetallics 17 (2009) 56.
[22] J.S.C. Jang, S.R. Jian, C.F. Chang, L.J. Chang, Y.C. Huang, T.H. Li, J.C. Huang, C.T. Liu, J. Alloys Compd. 478 (2009) 215.